JGR

Revisiting AVHRR tropospheric aerosol trends using principal component analysis

Jing Li[1,2], Barbara E. Carlson[1], and Andrew A. Lacis[1]

[1]NASA Goddard Institute for Space Studies, New York, New York, USA, [2]Department of Applied Physics and Applied Math, Columbia University, New York, New York, USA

Abstract The advanced very high resolution radiometer (AVHRR) satellite instruments provide a nearly 25 year continuous record of global aerosol properties over the ocean. It offers valuable insights into the long-term change in global aerosol loading. However, the AVHRR data record is heavily influenced by two volcanic eruptions, El Chichon on March 1982 and Mount Pinatubo on June 1991. The gradual decay of volcanic aerosols may last years after the eruption, which potentially masks the estimation of aerosol trends in the lower troposphere, especially those of anthropogenic origin. In this study, we show that a principal component analysis approach effectively captures the bulk of the spatial and temporal variability of volcanic aerosols into a single mode. The spatial pattern and time series of this mode provide a good match to the global distribution and decay of volcanic aerosols. We further reconstruct the data set by removing the volcanic aerosol component and reestimate the global and regional aerosol trends. Globally, the reconstructed data set reveals an increase of aerosol optical depth from 1985 to 1990 and decreasing trend from 1994 to 2006. Regionally, in the 1980s, positive trends are observed over the North Atlantic and North Arabian Sea, while negative tendencies are present off the West African coast and North Pacific. During the 1994 to 2006 period, the Gulf of Mexico, North Atlantic close to Europe, and North Africa exhibit negative trends, while the coastal regions of East and South Asia, the Sahel region, and South America show positive trends.

1. Introduction

Human activities associated with contemporary industrialization are believed to damage the climate system by releasing excessive amounts of trace gases and aerosols. In the understanding of global climate change, aerosols have been identified as one of the factors with largest uncertainty [*Intergovernmental Panel on Climate Change*, 2014]. Therefore, to quantify the climate effect of aerosols, it is essential to examine the long-term variability of their global distribution, especially the trends in their changing patterns. The recent retrospective reprocessing of historical satellite records from the advanced very high resolution radiometer (AVHRR) instruments provides a nearly 25 year long record of global aerosol and makes it possible to analyze long-term trends. *Mishchenko et al.* [2007] reported a likely decreasing trend of global mean aerosol optical depth after 1990. *Mishchenko and Geogdzhayev* [2007] further analyzed regional trends for both aerosol optical depth (AOD) and size information and indicated decreased aerosol loading over much of Europe, part of Atlantic, and increasing trends over western African coast. *Zhao et al.* [2008] used refined AVHRR Pathfinder Atmosphere-Extended aerosol retrieval to study long-term AOD trends and revealed similar global and regional trends. *Cermak et al.* [2010] also suggested a decrease in AOD since the early 1990s, which is consistent with the trend in surface solar radiation.

However, because of two volcanic eruptions—El Chichon on March 1982 and Mount Pinatubo on June 1991, the AVHRR aerosol record is also heavily influenced by volcanic aerosols, especially before the year 2000. These two events injected huge amounts of volcanic ash and sulfate aerosols into the atmosphere, and the resulting peaks in global AOD are well present in the AVHRR data [e.g., *Mishchenko et al.*, 2007; *Mishchenko and Geogdzhayev*, 2007]. The spatial structure and temporal evolution of volcanic aerosols have been studied by *Minnis et al.* [1993] and *Russell et al.* [1996] using AVHRR and Stratospheric Aerosol and Gas Experiment (SAGE) data. While previous studies on tropospheric aerosol trends excluded the first few years after the eruption, strong volcanic eruptions can inject large amount of sulfurous gases into the stratosphere, which form sulfate aerosols and can have a much longer-lasting effect. In particular, the gradual decay of volcanic aerosols from the eruption to background level may result in an overall downward trend in AOD, which masks the real trend of tropospheric aerosols. Moreover, due to the variability of volcanic aerosols both spatially and

temporally, a simple correction to the globally or regionally averaged time series is not appropriate. To better estimate the tropospheric aerosol trends, especially those of anthropogenic origin, this contamination by volcanic aerosols should be taken into account in both the space and time dimensions. In this study, we show that a principal component analysis (PCA) decomposition of the AVHRR data can successfully separate the variability of volcanic aerosols from that of the tropospheric aerosols. The effectiveness of this technique should be primarily attributed to the relatively independent physical mechanisms associated with stratospheric and tropospheric aerosols. The spatial distribution and temporal variability of the volcanic aerosol component are further verified using stratospheric aerosol optical depth derived from the Stratospheric Aerosol and Gas Experiment II data. The tropospheric aerosol variability is also confirmed by comparing with Moderate Resolution Imaging Spectroradiometer (MODIS) and Multiangle Imaging Spectroradiometer (MISR) AOD for the common data period (i.e., after 2000) using combined principal component analysis (CPCA) [e.g., *Bretherton et al.*, 1992; *Li et al.*, 2013a]. We further reconstruct the data set by removing the volcanic aerosol component in order to better estimate the tropospheric aerosol trends. The reconstructed globally averaged monthly mean AOD suggests an increasing trend in the 1980s, consistent with *Mishchenko et al.* [2007], while the trend after 1990 becomes almost flat. AOD trend maps showing regional differences are also presented and discussed.

The paper is organized as follows: the data and methods used in the study are introduced in section 2. Section 3 presents the results of PCA analysis and trend estimate. Some discussions and conclusions are given in the final section.

2. Data and Methods

2.1. Data

The AVHRR AOD data set used in this study is obtained from the nominal Global Aerosol Climatology Project (GACP), available at http://gacp.giss.nasa.gov. The aerosol product is derived from the International Satellite Cloud Climatology Project DX radiance data set composed of calibrated and sampled channels 1 and 2 AVHRR radiances [*Rossow and Garder*, 1993; *Rossow and Schiffer*, 1999]. The detailed aerosol retrieval algorithm can be found in *Mishchenko et al.* [1999] and *Geogdzhayev et al.* [2002, 2005]. The aerosol optical depth data reported by the GACP is at 550 nm. The data are reported as monthly means gridded at a spatial resolution of $1° \times 1°$. The temporal coverage for the data used here is January 1982 to June 2006. *Liu et al.* [2004] validated the AVHRR aerosol retrieval against shipborne Sun photometer data and reported an 11% overestimation with a random error of 0.04.

In addition, to verify the PCA components of volcanic and tropospheric aerosols, aerosol data from the SAGE II, MODIS, and MISR instruments are also used. The SAGE II instrument [*Mauldin et al.*, 1986; *McCormick*, 1987] provides unique information of aerosol properties in the stratosphere. It had been continuously measuring the aerosol extinction profiles at four wavelengths from October 1984 to August 2005. Here we use the version 7.00 SAGE II monthly extinction profile data (available at https://eosweb.larc.nasa.gov/) at 525 nm from January 1985 to December 2004. The SAGE product reports tropopause height for each profile; we therefore integrate each aerosol extinction profile above the tropopause level to calculate stratospheric optical depth. Due to the sparse latitude-longitude sampling of the SAGE instrument, particularly evident in the tropics, we applied nearest neighbor interpolation to map the SAGE AOD into $1° \times 1°$ grid boxes and temporally average the SAGE data to better compare the spatial patterns with AVHRR. Therefore, for this comparison, the SAGE data are presented as a temporally averaged spatial map and a global mean time series, and the comparison is more qualitative than quantitative due to these important sampling differences.

MODIS and MISR are two more recent satellite sensors that retrieve aerosol optical properties. Their data records begin after 2000 when stratospheric aerosols were reduced to background levels. Also, these two instruments use multiple channels and sophisticated retrieval algorithms [e.g., *Martonchik et al.*, 2009; *Remer et al.*, 2008; *Levy et al.*, 2007] and have the advantage in spatial resolution, sensitivity, and radiometric calibration [*Geogdzhayev et al.*, 2004; *Mishchenko et al.*, 2007]. They yield better retrieval accuracy compared with AVHRR. The reported uncertainty of ocean retrievals are $\pm 0.03 \pm 0.05 \times$ AOD for MODIS [*Remer et al.*, 2008; *Levy et al.*, 2007] and ± 0.03 or $\pm 0.1 \times$ Aerosol Robotic Network AOD for MISR [*Kahn et al.*, 2010]. Therefore, a comparison of the spatial-temporal modes of variability between these two data sets and AVHRR is also performed, in order to verify the tropospheric aerosol components from the AVHRR data. Here we use the Level 3 monthly mean MODIS and MISR data both from the EOS-Terra platform from March 2000 to June
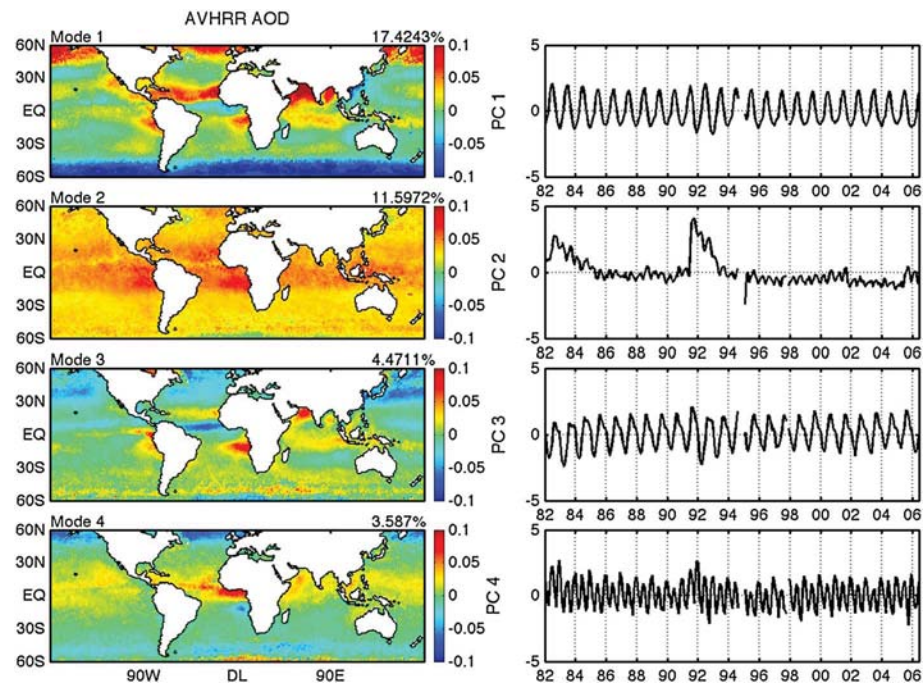
Figure 1. PCA analysis of the full AVHRR AOD record. The number on the top right corner of the spatial map indicates the percentage of variance explained by this mode. Mode 2 captures the variability of volcanic aerosols.

2006. Only ocean data are used to be consistent with AVHRR. The MODIS data resolution is 1° × 1°, while the MISR data is downgraded from the original 0.5° × 0.5° resolution to 1° × 1°.

2.2. Method

The PCA method, also known as principal component analysis, is widely used to extract leading orthogonal modes of variability in multidimensional data. It finds the orthogonal components by decomposing the data covariance matrix into a set of independent eigenvectors, with the first eigenvector explaining the most variance, the second explaining most of the remaining variance, and so on. A detailed description and implementation of this method can be found in *Bjornsson and Venegas* [1997]. Examples applying PCA analysis to aerosol data are presented by *Li et al.* [2009a, 2011, 2013b]. *Li et al.* [2009b, 2013a] indicate that many aerosol source regions that are governed by different emission and transport mechanisms and meteorological conditions can be isolated into different orthogonal modes by the PCA. Because volcanic aerosols are generally produced by sporadic eruptions, and can reach the stratosphere, where their interference with human activities, meteorological, and climatological conditions are minimal, we consider that this technique has the potential to separate the variability of volcanic aerosols from the other tropospheric aerosol species. Nonetheless, some mechanisms, such as large-scale circulation, may affect the transport, and thus, the spatial distribution of both volcanic aerosols and tropospheric aerosols, which will result in signal, overlaps in the orthogonal modes. This issue will be discussed further in the results section.

To verify the PCA modes of AVHRR data that represent tropospheric aerosols, we apply the combined principal component analysis [*Kutzbach*, 1967; *Bretherton et al.*, 1992] on MODIS, MISR, and AVHRR data after the year 2000. This method extracts the common modes of variability from different data sets. Specifically, the three $N \times M$ AOD data fields from MODIS, MISR, and AVHRR are combined to form a large data matrix of size $3 N \times M$, where N is the number of spatial locations and M is the number of observations at each location for each data set. Regular PCA analysis is then performed on this combined field. The procedure is the same as PCA, and mathematical descriptions can be found in *Li et al.* [2013b]. In this way, the leading modes will maximize the variance explained by the sum of the elements in the combined field. Each mode from the decomposition of the combined covariance matrix is composed of a spatial pattern of each data set and a shared time series. The three spatial patterns of each mode can be viewed as the projection of the associated

time series on each of the three data sets, respectively. The same as PCA, the leading CPCA modes also account for most of the variance in all the three data sets, which represent major spatial-temporal variability. Therefore, the agreement on the variability within different data sets is examined by comparing the spatial patterns from the dominant modes. Furthermore, as the variability during the "volcano-free" period reflects that of the tropospheric aerosols, the comparison between the CPCA modes during the volcano-free period and the PCA modes from the volcano-affected period excluding the volcanic aerosol mode suggests that these modes represent tropospheric aerosol variability. For example, if one or more dominant modes extracted from the volcano-affected period agree with the modes from volcano-free period in both the spatial pattern and time series, we are able to conclude that these modes from the volcano-affected period mainly represent tropospheric aerosol variability with minimal influence of volcanic aerosols.

3. Results

3.1. PCA Analysis of AVHRR Data

The PCA analysis is first performed on the full AVHRR AOD data record. Figure 1 shows the first four modes of the full data record. The spatial pattern of Mode 2 has near uniform global distribution, and its time series has two strong peaks in 1982 and 1991, respectively. Both features suggest that it is associated with volcanic aerosols. This mode accounts for more than 10% of the total variance, which implies that volcanic aerosols are an important component in the AVHRR data record. However, because the eruption of Mount Pinatubo is much more intense than El Chichon [e.g., *Bluth et al.*, 1992; *Strong and Stowe*, 1993], the peak in 1992 is almost twice as large as that in 1982 and the spatial signal of Mode 2 mostly concentrates around the tropics where Pinatubo is located, and the variability of El Chichon eruption is not full captured. As a result, we also repeat the analysis on the two periods after the two volcanic eruptions separately, to best extract the signal of each volcano. Figures 2a and 2b present the four leading modes for the periods 1982–1990 and 1991–2006. Now it is clearly seen that positive anomalies in Mode 2 of Figure 2a are distributed more northward compared to Figure 2b, which is due to the fact that El Chichon is located in the Northern Hemisphere (Mexico), while Pinatubo is located at the equator (Philippines). The magnitude and variance explained by the Pinatubo mode are also larger than those of the El Chichon mode.

Studies have shown that the Pinatubo eruption released nearly 3 times the amount of SO_2 compared to the El Chichon based on Total Ozone Mapping Spectrometer [*Heath et al.*, 1975] measurements [*Krueger*, 1985; *Bluth et al.*, 1992]. The SO_2 clouds were distributed around the whole tropical area in 2 weeks. As this time scale is not resolved in the monthly mean data, only a uniform distribution global pattern is reflected. The aerosol amount introduced by the Pinatubo into the stratosphere is almost twice as large as that of the El Chichon [*Strong and Stowe*, 1993]. Moreover, the SO_2 and aerosols from Pinatubo are also longer lasting than those from El Chichon, which results in a longer decay time. Finally, it is worth noting that the time series of both volcanic aerosol modes exhibit some seasonal variability. *Post et al.* [1996] showed the similar seasonality between the stratospheric transportation of El Chichon and Pinatubo measurements using lidar observations and indicated that seasonal atmospheric dynamics play a key role in both the poleward dispersion and subsidence of stratospheric aerosols. Nonetheless, the poleward transport of volcanic aerosols is also influenced by the quasi-biennial oscillation [*Trepte et al.*, 1993], which is not exactly seasonal.

In order to verify that Mode 2 represents volcanic aerosols, we compare this mode with the SAGE II data. Figure 3 shows the overall monthly mean map averaged from 1985 to 2004 and globally averaged time series of SAGE II 525 nm optical depth. As the SAGE II AOD is calculated by integrating extinction coefficients above the tropopause, Figure 3 represents the time period mean spatial distribution and the globally averaged temporal variability of stratospheric aerosols. As SAGE II does not cover the El Chichon eruption, the comparison is focused on the Pinatubo period. The spatial pattern of AVHRR Mode 2 in Figure 2b highly resembles that of SAGE II, with most of the aerosol signal in the tropics, but also some in the polar region due to the poleward transport in the stratosphere [*Trepte et al.*, 1993]. The correlation (Here and in the rest of the paper, correlation refers to Pearson's correlation.) between the spatial pattern of AVHRR Mode 2 (Figure 2b) and SAGE II AOD is 0.52. Nonetheless, there are still some differences between SAGE II AOD and AVHRR Mode 2. In addition to the tropical belt, SAGE II AOD also has relatively high concentrations near polar regions. This should be related to the Brewer-Dobson circulation. AVHRR also appears to be slightly influenced by aerosol transport from south Africa and South America. This might be due to similar transport patterns between
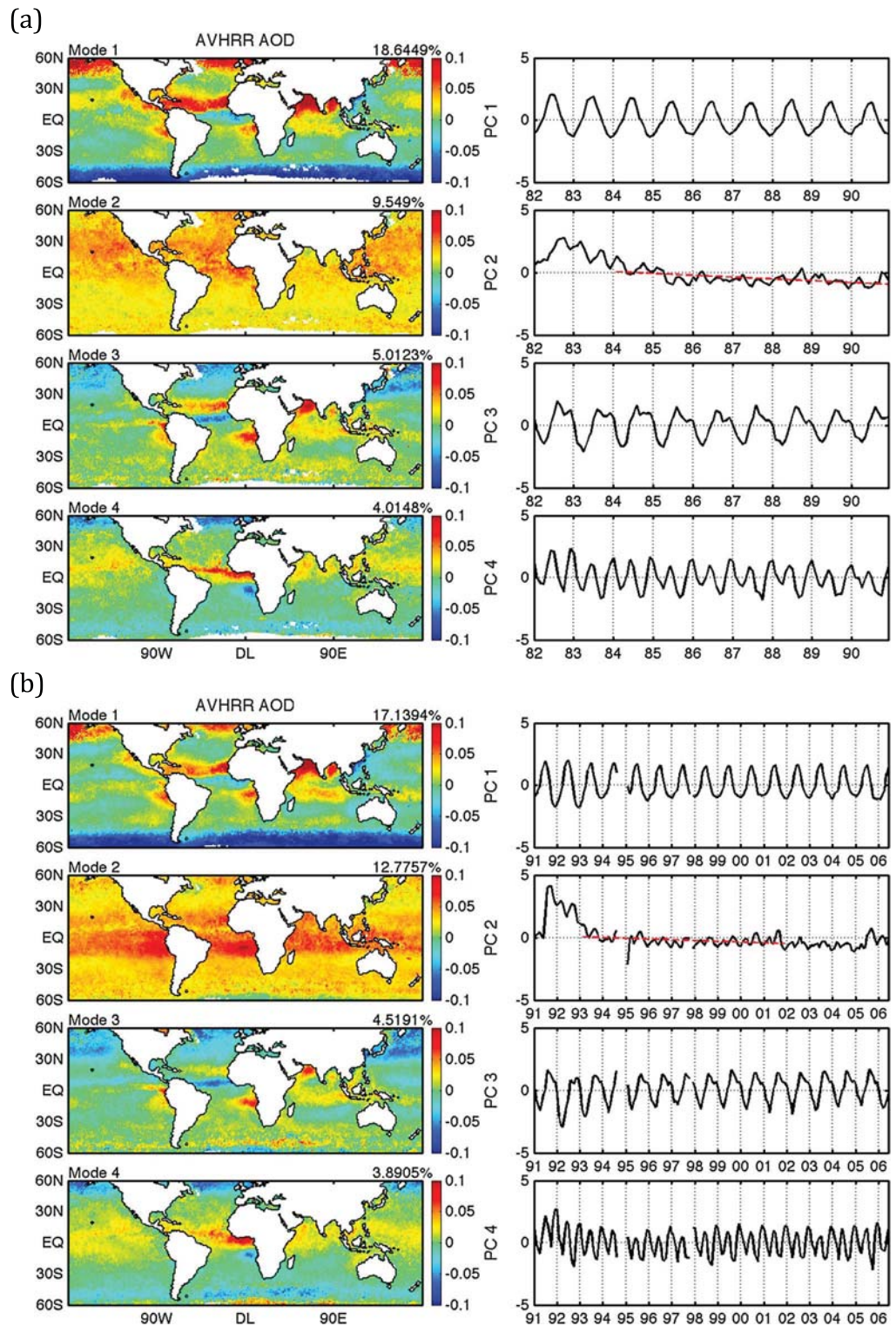
Figure 2. The four leading PCA modes of AVHRR AOD for the periods (a) 1982–1990 and (b) 1991–2006. These two periods are heavily influenced by two volcano eruptions: El Chichon on March 1982 and Mount Pinatubo on June 1991. The second mode captures volcanic aerosols. The red dashed line in PC 2 shows the decreasing trend of volcanic aerosol decay after the eruption, which can last as long as 10 years.
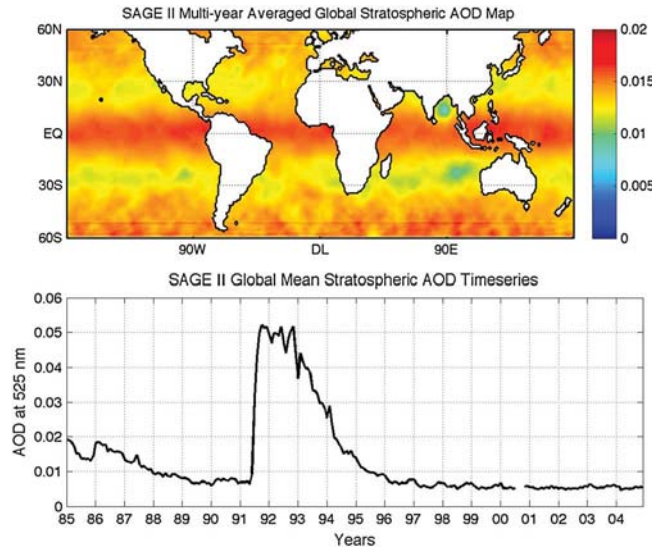
Figure 3. Multiyear averaged global AOD distribution and global mean time series of SAGE II AOD, integrated above the tropopause. The spatial pattern is similar to that of Mode 2 in Figure 2b with 0.52 correlation. And the correlation between SAGE global mean AOD and AVHRR PC 2 for the period 1991–2004 is 0.85. These agreements indicate that PCA analysis separates volcanic aerosol variability.

tropospheric and volcanic aerosols in the tropical region, which means that part of their signals are not orthogonal and thus not completely separated by the PCA analysis. The global mean time series of SAGE II AOD is also very similar to the AVHRR principal component (PC) 2 in Figure 2b. The correlation between these two series from 1991 to 2004 is 0.85. Some seasonal variability in the PC 2 of the AVHRR data can also be explained by the contamination of some tropospheric aerosols. A closer examination of the seasonality in PC 2 indicates that it mostly exhibits semiannual features, with high peak in boreal fall and a secondary peak in boreal spring. The positive signals over the tropics are also mixed with aerosol transport from South America and

Africa. As these aerosol transport patterns have similar spatial structure (extending over the tropics) as volcanic aerosols, some of their seasonality are captured in Mode 2 rather than completely separated into other modes.

Next, we will examine Modes 1, 3, and 4 of the AVHRR data and provide evidence that they represent aerosol variability in the troposphere. This is accomplished by comparing these three modes with the leading three modes in the CPCA analysis of MODIS, MISR, and AVHRR AOD during the February 2000 to June 2006 period (Figure 4). During this period, volcanic aerosols have reduced to background level [*Thomason et al.*, 2008], and therefore, the major PCA modes should be associated with tropospheric aerosols. First of all, the CPCA results in Figure 4 reveal excellent agreement across the three data sets in all three modes. The correlations between the spatial patterns of Modes 1–3 of AVHRR and MODIS are 0.80, 0.56, and 0.56, respectively, and those between AVHRR and MISR are 0.76, 0.53, and 0.53, respectively. This is good support that the AVHRR instrument well captures global aerosol variability over the oceans, despite the fact that its retrieval algorithm
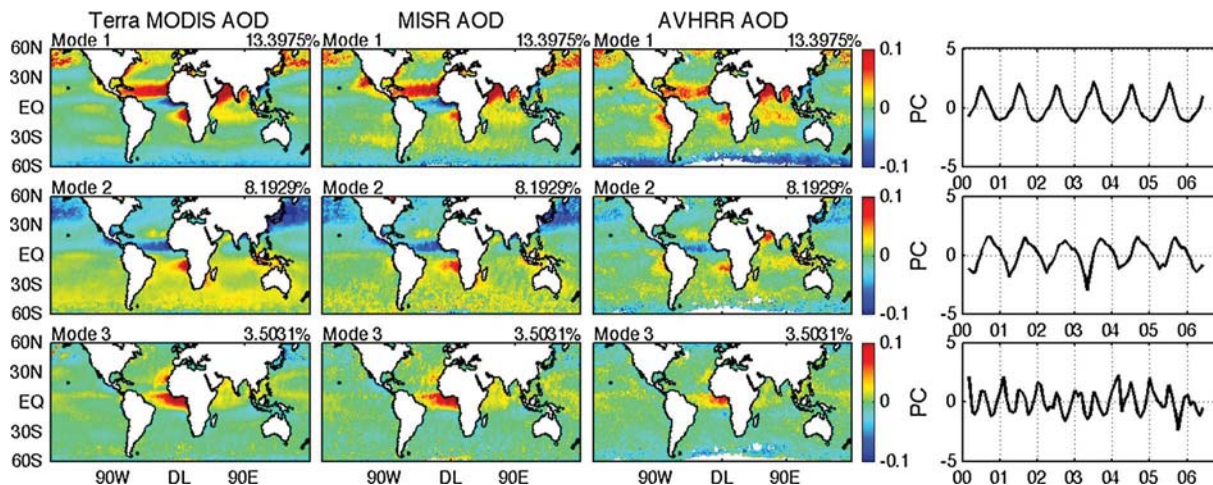

Figure 4. CPCA analysis of MODIS, MISR, and AVHRR data for the volcano-free period of 2000–2006. The spatial pattern of AVHRR well agrees with that of MISR and MODIS, indicating the reliability of AVHRR AOD retrievals. Moreover, these three patterns highly resemble Modes 1, 3, and 4 of Figures 1a and 1b. This is a strong evidence that these three modes in Figure 1 represent tropospheric aerosols and further support the effectiveness of PCA analysis in separating tropospheric and volcanic aerosols.
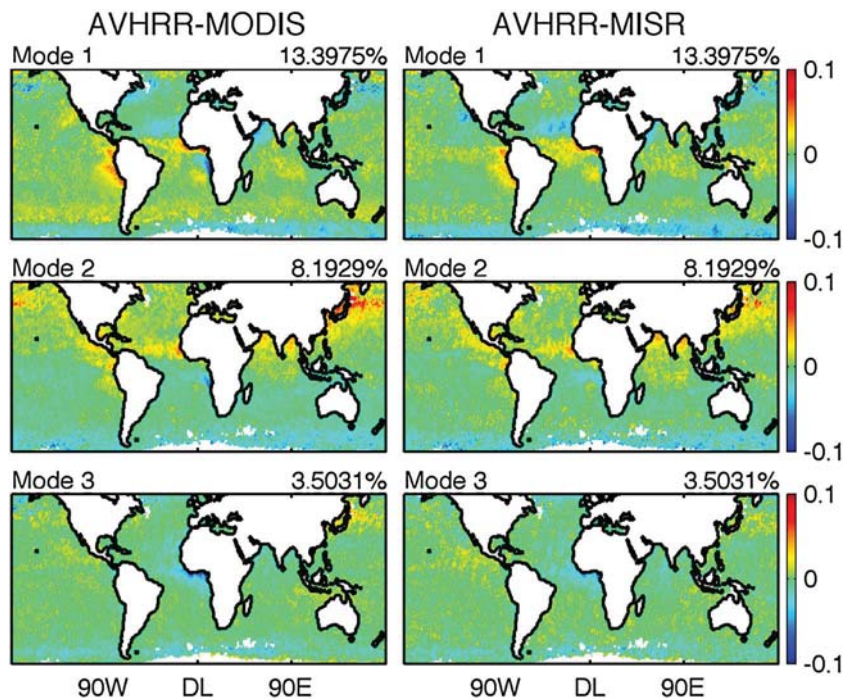
Figure 5. Difference between Modes 1–3 of AVHRR data and (left column) MODIS and (right column) MISR. The difference is calculated as AVHRR mode minus MODIS/MISR mode.

and instrumental design are not as sophisticated as MODIS and MISR. We also compare the magnitude of the spatial patterns by examining the difference between AVHRR and MODIS/MISR, respectively. The difference maps for the three spatial patterns are shown in Figure 5. Nonetheless, AVHRR still has some overall lower variability; i.e., the AVHRR signals are, in general, weaker with negative biases over the regions of positive signal, such as West Africa in Mode 1 and Sahel region in Mode 3 and positive biases over regions of negative signal, such as North Pacific in Mode 2. Considering instrumental and algorithmic differences, this bias in AVHRR is reasonable. Moreover, comparing Figure 2 and Figure 4, we can clearly see that the spatial patterns of Modes 1–3 of Figure 4 are almost identical to those of Modes 1, 3, and 4 of Figures 2a and 2b. In fact, the correlation coefficients between Modes 1–3 of Figure 4 and Modes 1, 3, and 4 of Figure 2a are 0.72, 0.60, and 0.54, respectively, and the correlation coefficients between Modes 1–3 of Figure 4 and Modes 1, 3, and 4 of Figure 2b are 0.91, 0.75, and 0.74, respectively. The time series between the three pairs are also in phase, with the first modes showing a winter-summer seasonal cycle, the second one with a spring-fall seasonal cycle, and the third one exhibiting semiannual variability with a major peak in boreal winter and a secondary peak in boreal summer. Since Figure 4 is decomposed using data from volcano-free period, it is dominated by the variability of tropospheric aerosols. This consistency between Figure 4 and Modes 1, 3, and 4 of Figure 2 is a strong indication that PCA analysis of the AVHRR data during the volcano-affected periods effectively separates the variability of the other tropospheric aerosol species from that of volcanic aerosols.

In summary, the agreement between Mode 2 of AVHRR and SAGE II, and between Modes 1, 3, and 4 and leading modes from the volcano-free period, well demonstrate the effectiveness of the PCA method in separating volcanic and tropospheric aerosols. The reliability of the AVHRR data is also corroborated through comparison with MODIS and MISR using the CPCA method. Finally, it should be noted that the PC 2 of both periods 1982–1990 and 1991–2006 have decreasing trends which last as long as 10 years after the eruption (red dashed lines in Figure 1). We suspect that this trend likely leads to a negative bias in the estimation of tropospheric aerosol trends using the full data set.

3.2. Trend Analysis

As the original data set can be reproduced by the sum of the product of each spatial mode, PC, and eigenvalue, we are able to generate a "reduced" data set by removing certain components. In this section, we
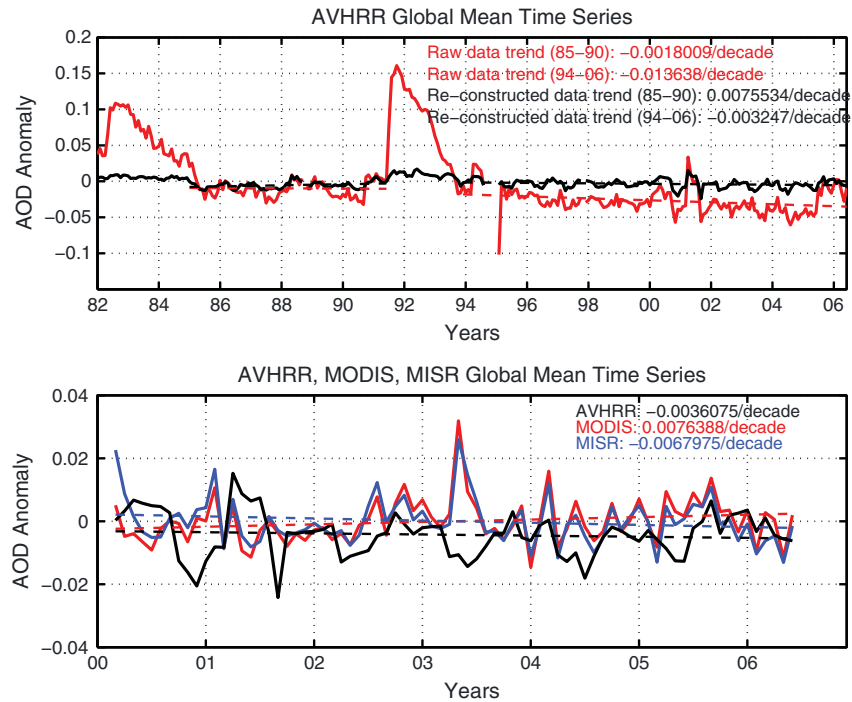
Figure 6. (top) Comparison of the global mean time series of AVHRR global mean aerosol topical depth anomaly time series (red line) and the time series of AVHRR tropospheric aerosol proxy after removing the volcanic aerosol component (black line). The associated trend lines are shown as red and black dashed lines, respectively. Globally, there is a small insignificant increasing trend from 1985 to 1990 and a significant decreasing trend from 1994 to 2006. (bottom) The aerosol optical depth anomalies and trends from 2000 to 2006 from MODIS, MISR, and AVHRR. None of the trends are statistically significant.

construct a "tropospheric aerosol proxy" from the full AVHRR data set by removing the volcano-dominated aerosol mode (Mode 2) for both of the two periods. This will allow better examination of tropospheric aerosols, especially those associated with anthropogenic activities.

With this tropospheric aerosol proxy data set, we reestimate both the global and regional AOD trends. Figure 6 shows the comparison of the globally averaged monthly mean anomaly time series of the AVHRR AOD data (red lines) and the reconstructed data (black line) and the associated linear trends (red and black dashed lines, respectively). The anomaly time series is constructed by removing the multiyear averaged seasonal cycle. The linear trends are estimated by performing a linear regression of the time series against the months. We use Student's t test to estimate the statistical significance of the trends. Since the degrees of freedom used in the significance calculation are influenced by the autocorrelation of each of these two time series, we adjusted the degrees of freedom following *Bretherton et al.* [1999],

$$T^* = \frac{1 - r_1 r_2}{1 + r_1 r_2} T$$

where T^* is the degree of freedom used in the significance calculation, r_1, r_2 are the lag-one autocorrelation of each time series, and T is the unadjusted number of the degrees of freedom. In this paper, the trends are considered significant if they pass a 5% significance level test, with the null hypothesis of no significant trend. By comparing the raw and reconstructed data in Figure 6, the effect of removing PCA Mode 2 is quite clear: the two strong peaks in 1983 and 1991 are greatly reduced (note the *y* axis scale change), and the downward tendencies after the two volcanic eruptions are mitigated; i.e., the trend from 1985 to 1990 shifts from negative to insignificant and the negative trend from 1994 to 2006 becomes smaller in the reconstructed data. Although the tropospheric proxy data set removes the bulk of the volcanic aerosol signal, some residual still exists as mentioned in section 3.1. This has two effects on the reconstructed time series: (1) the time series is still perturbed with a positive anomaly during the first 3 years of volcanic eruptions and (2) the variability in the reconstructed data set during the volcano-free period is slightly smaller than that in the raw data, as a small fraction of tropospheric aerosol variability is captured by Mode 2 which has been removed. Therefore,
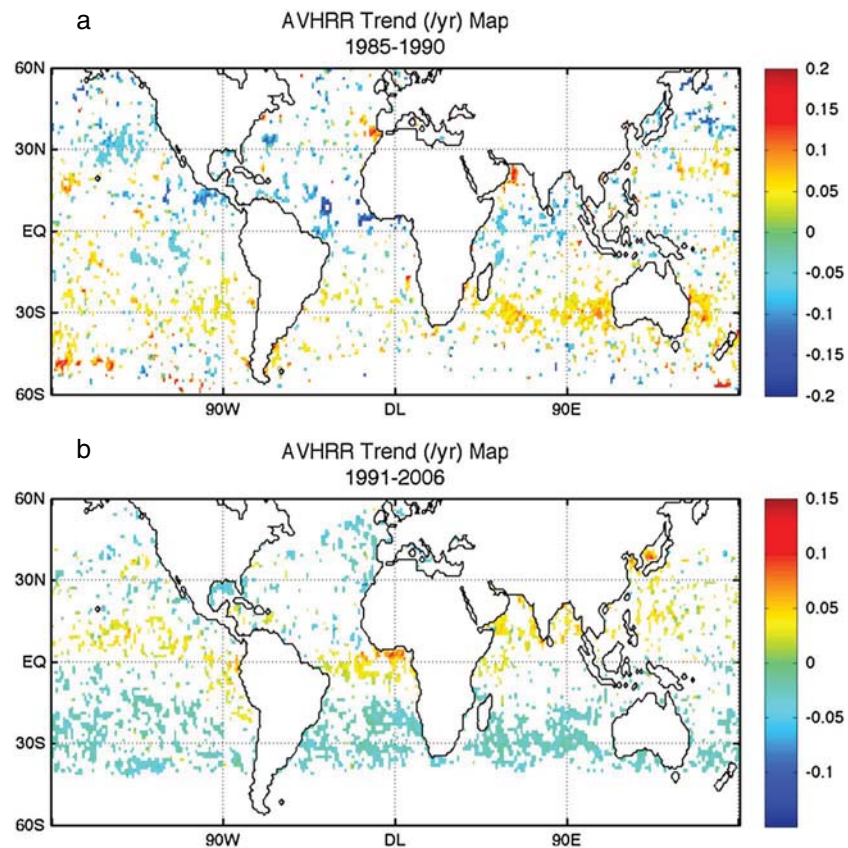
Figure 7. Maps showing linear trend at each grid box from the reconstructed AVHRR AOD data set for the periods (a) 1985–1990 and (b) 1991–2006. Only trends at 5% significance level or above are shown. During the period 1985 to 1990, negative trends are found off West African coast and North Pacific, and positive trends mostly come from North African coast and the Arabian Sea. From 1991 to 2006, AOD increased over majority of Asia, and biomass burning regions of South America and south Africa, while decreased over North Atlantic and North Africa.

linear regression is performed 3 years after the eruption to exclude the immediate effect of volcanic aerosols. However, the PCA analysis does remove potential bias in the trend caused by the decay of volcanic aerosols up to 10 years after the eruption. In the 1980s, we only observe an insignificant trend, which has a p value of 0.316 when tested using the Student's t test of the linear regression slope. An earlier study by *Zhao et al.* [2008] indicated a negative trend in the AVHRR AOD record. The different trend found here should be attributed to the removal of the volcanic aerosol signal. During the period 1994 to 2006, even excluding the variability of volcanic aerosols, the global AOD still exhibits a negative trend of −0.0032/decade, and this trend is significant at the 5% significance level, associated with a p value of 0.0192. The sign of this trend is still consistent with the decreasing trends indicated by *Mishchenko et al.* [2007], albeit with a smaller magnitude due to the removal of some volcanic aerosol residuals. It also agrees with the "global brightening" trend, which is attributed to decrease in aerosol loading. Finally, to compare with MODIS and MISR, the time series for the volcano-free period of 2000 to 2006 is also analyzed when MODIS and MISR data become available. During this period, MISR and AVHRR have small negative trends, while MODIS exhibits a small positive trend. However, none of these three trends are statistically significant. The insignificant global trends in MODIS and MISR data agree with the results of a previous study by *Zhang and Reid* [2010]. The p values are 0.106, 0.141, and 0.423 for MODIS, MISR, and AVHRR trends, respectively. Compared with the raw time series that has a much larger downward tendency during this period, the trend of the reconstructed time series agrees better with MODIS and MISR.

In order to further examine the spatial distribution of the trends, we plotted the linear trend for each valid grid box for the two periods in Figure 7. A grid box is considered valid only if there are more than 60 monthly mean data points in its entire record. Consistent with global mean results, the trends for each grid box are

estimated by a linear regression on the anomaly time series constructed by removing the multiyear averaged seasonal cycle. Student's t test is performed to calculate the significance level of the linear regression slope, and only statistically significant ($>$5% significance level) trends are shown on the maps. Figure 7 indicates that there are considerable spatial differences in the trends and between the two periods. In the 1980s, a negative trend as large as -0.2/decade is found over the West African coast and tropical Atlantic, which should be related to biomass burning aerosols. Negative trends also appear over the North Pacific. Positive trends are found over the North Arabian Sea, suggesting an increase in dust aerosols over the Arabian Peninsula and around Australia. Between 1994 and 2006, AOD increased over coastal regions off East, Southeast, and South Asia. Increase in aerosol loading over East Asia until around 2005 is also reported by *Lu et al.* [2010] and *Streets et al.* [2006], who attributed the results to the economic development of China. Positive trends are also found for aerosols transported from South America and the Sahel, which might be due to an increase in biomass burning during this period. Negative trends are mostly found over North Atlantic and the North African coast, which are associated with aerosol transport from Northeast America, Europe, and the Sahara. The regional trends from 1994 to 2006 are consistent with previous studies using visibility measurements [*Wang et al.*, 2009; *Mahowald et al.*, 2007]. They are also consistent with the surface brightening trend over the U.S. and Europe, but dimming over Southeast Asia and India [*Wild et al.*, 2005, 2009] since 1990. Moreover, *Chin et al.* [2013] also found increased aerosol loading over East and South Asia and decreases over dust-dominated regions by combining observations and model outputs. They also indicated that the aerosol trends are in line with emission changes.

4. Discussions and Conclusions

In this study, we used AVHRR AOD data as an example of the ability of PCA analysis to separate the variability of volcanic aerosols and the other tropospheric aerosol species. This attempt is successful mainly because of the relatively independent sources, transportation, and distribution features of these two aerosol types. Strong volcanic eruptions, such as the El Chichon and Mount Pinatubo, emit large amount of sulfurous gases, which can reach high altitudes and form sulfate particles. They tend to have long-lasting, near-uniform global distribution. While most of the tropospheric aerosol species are generated through various human activities or persistent natural processes, they generally concentrate in the lower troposphere and are heavily influenced by meteorological conditions; therefore, they have shorter lifetimes and more localized distributions. Nonetheless, there are still some overlaps in the signal of volcanic and tropospheric aerosols, for example, during the period shortly after the volcano eruption, tropospheric AOD is also increased. In addition, some tropospheric aerosols, such as dust and smoke, can also be transported to high altitudes and thus have extensive spatial distributions. Sulfate aerosols from anthropogenic sources and other natural sources, such as dimethyl sulfide, are also believed to contribute to stratospheric aerosols. These nonindependent components should be responsible for the large variability during the first 3 years after the volcanic eruption of PCs 1, 3, and 4 and some contamination of tropospheric aerosols in Mode 2. Another limitation of removing the volcanic aerosol signal using PCA is that we are assuming constant spatial distribution with a time-varying loading. While the spatial pattern of Mode 2 highly resembles that of the SAGE II AOD, the spatial distribution of volcanic aerosol does have short-term change from initial eruption to global distribution and long-term change due to poleward transportation by the stratospheric circulation. In the current study, however, these factors are not significant since we are using monthly mean data and excluding polar regions. These limitations and uncertainties should be noted when interpreting the PCA results and trend analysis. While instruments such as SAGE II provide independent measurements of stratospheric aerosols, the PCA technique offers a potential to remove long-term bias caused by volcanic aerosol decay from column aerosol retrievals from the same data set, especially if stratospheric aerosol measurements are not available or if different instruments have other sources of uncertainty such as calibration issues.

In addition to the decay of volcanic aerosols, it should be noted that there are also other sources of uncertainty that result in the error in the AOD trend estimate. *Li et al.* [2009b] investigated the influence of several factors on satellite aerosol retrieval, including calibration, cloud screening, aerosol models and surface effects, and estimated ranges of uncertainty using the AVHRR data. Recently, *Mishchenko et al.* [2012] conducted a sensitivity study of AVHRR AOD retrieval using nonconstant imaginary refractive indices and found that the decreasing trend vanishes when the imaginary part increases from 0.003 at the beginning of the record to 0.007 to the end of the record.

By removing the mode representing volcanic aerosols, we are attempting to minimize the signal of volcanic aerosol decay in estimating tropospheric aerosol trends. Recent studies suggested increases in stratospheric AOD after 2002, possibly due to small volcanic eruptions [*Vernier et al.*, 2011; *Solomon et al.*, 2011], and indicated that this trend may lead to the slowdown of global warming observed in the past decade. On the other hand, other studies suggest that the slowdown in global warming can mainly be attributed to heat absorption by the deep ocean [*Katsman and van Oldenborgh*, 2011; *Meehl et al.*, 2011; *Guemas et al.*, 2013]. As AVHRR data have true global coverage while most of the studies on stratospheric aerosol trends either use lidar profile measurements at a specific location, or SAGE or CALIPSO data, which have limited spatial sampling, it is worth examining any trends in the AVHRR PC 2, which represents most of the stratospheric aerosol variability. From the results, we do not observe significant increases in aerosol loading after 2002.

Overall, our study offers a different approach to assessing tropospheric aerosol trends using the AVHRR data by separating different modes of variability in the data. The major conclusions are summarized as follows:

1. PCA analysis separates the variability of volcanic aerosols and tropospheric aerosols into different spatial-temporal modes.
2. The identification of a mode representing volcanic aerosol variability is supported through comparison with SAGE II AOD data. The modes representing tropospheric aerosols during the volcano-affected period are verified through comparison with the CPCA modes of MODIS, MISR, and AVHRR during the volcano-free period.
3. The agreement between CPCA modes of AVHRR with those of MODIS and MISR confirms the reliability of AVHRR AOD retrieval.
4. The global trends estimated using the reconstructed data after the removal of the volcanic aerosol component suggest a significant negative trend from 1994 to 2006, while no significant trend is found for the earlier period.
5. Regionally, for the period of 1985 to 1990, negative trends are found over West African coast and the North Pacific, while positive trends mainly come from the dust transport regions of the North Atlantic and the Arabian Sea. From 1994 to 2006, AOD decreased over most of the North Atlantic, while it increased over East and South Asia and the ocean regions off the South American and south African coasts.

References

Bjornsson, H., and S. A. Venegas (1997), A manual for EOF and SVD analysis of climate data, CCGCR Rep. 97-1, McGill Univ., Montréal, QC, Canada, 52 pp.

Bluth, G. J., S. D. Doiron, C. C. Schnetzler, A. J. Krueger, and L. S. Walter (1992), Global tracking of the SO2 clouds from the June, 1991 Mount Pinatubo eruptions, *Geophys. Res. Lett.*, *19*(2), 151–154.

Bretherton, C. S., C. Smith, and J. M. Wallace (1992), An intercomparison of methods for finding coupled patterns in climate data, *J. Clim.*, *5*(6), 541–560.

Bretherton, C. S., M. Widmann, V. P. Dymnikov, J. M. Wallace, and I. Bladé (1999), The effective number of spatial degrees of freedom of a time-varying field, *J. Clim.*, *12*, 1990–2009.

Cermak, J., M. Wild, R. Knutti, M. I. Mishchenko, and A. K. Heidinger (2010), Consistency of global satellite-derived aerosol and cloud data sets with recent brightening observations, *Geophys. Res. Lett.*, *37*, L21704, doi:10.1029/2010GL044632.

Chin, M., et al. (2013), Multi-decadal variations of atmospheric aerosols from 1980 to 2009: Sources and regional trends, *Atmos. Chem. Phys. Discuss.*, *13*, 19,751–19,835, doi:10.5194/acpd-13-19751-2013.

Geogdzhayev, I. V., M. I. Mishchenko, W. B. Rossow, B. Cairns, and A. A. Lacis (2002), Global two-channel AVHRR retrievals of aerosol properties over the ocean for the period of NOAA-9 observations and preliminary retrievals using NOAA-7 and NOAA-11 data, *J. Atmos. Sci.*, *59*(3), 262–278.

Geogdzhayev, I. V., M. I. Mishchenko, L. Liu, and L. Remer (2004), Global two-channel AVHRR aerosol climatology: Effects of stratospheric aerosols and preliminary comparisons with MODIS and MISR retrievals, *J. Quant. Spectrosc. Radiat. Transfer*, *88*, 47–59, doi:10.1016/j.jqsrt.2004.03.024.

Geogdzhayev, I. V., M. I. Mishchenko, E. I. Terez, G. A. Terez, and G. K. Gushchin (2005), Regional advanced very high resolution radiometer–derived climatology of aerosol optical thickness and size, *J. Geophys. Res.*, *110*, D23205, doi:10.1029/2005JD006170.

Guemas, V., F. J. Doblas-Reyes, I. Andreu-Burillo, and M. Asif (2013), Retrospective prediction of the global warming slowdown in the past decade, *Nat. Clim. Change*, *3*, 649–653, doi:10.1038/nclimate1863.

Heath, D. F., A. J. Krueger, H. A. Roeder, and B. D. Henderson (1975), "The solar backscatter ultraviolet and total ozone mapping spectrometer (SBUV/TOMS) for Nimbus G.", *Opt. Eng.*, *14*(4), 144,323-144,323.

IPCC (2014), Working group I contribution to the IPCC fifth assessment report (AR5), climate change 2014: The physical science basis.

Kahn, R. A., B. J. Gaitley, M. J. Garay, D. J. Diner, T. F. Eck, A. Smirnov, and B. N. Holben (2010), Multiangle Imaging SpectroRadiometer global aerosol product assessment by comparison with the Aerosol Robotic Network, *J. Geophys. Res.*, *115*, D23209, doi:10.1029/2010JD014601.

Katsman, C. A., and G. J. van Oldenborgh (2011), Tracing the upper ocean's missing heat. *Geophys. Res. Lett.*, *38*, L14610, doi:10.1029/2011GL048417.

Krueger, A. J. (1985), Detection of volcanic eruptions form space by their sulfur dioxide clouds, *American Institute of Aeronautics and Astronautics 23rd Aerospace Sciences Meeting*, AIAA-85-0100, Reno, Nevada, 5 pp., January 14-17.

Kutzbach, J. (1967), Empirical eigenvectors in sea-level pressure, surface temperature, and precipitation complexes over North America, *J. Appl. Meteorol.*, *6*, 791–802.

Levy, R. C., L. A. Remer, and O. Dubovik (2007), Global aerosol optical properties and application to Moderate Resolution Imaging Spectroradiometer aerosol retrieval over land, *J. Geophys. Res.*, *112*, D13210, doi:10.1029/2006JD007815.

Li, J., B. E. Carlson, and A. A. Lacis (2009a), A study on the temporal and spatial variability of absorbing aerosols using Total Ozone Mapping Spectrometer and Ozone Monitoring Instrument Aerosol Index data, *J. Geophys. Res.*, *114*, D09213, doi:10.1029/2008JD011278.

Li, Z., X. Zhao, R. Kahn, M. Mishchenko, L. Remer, K. H. Lee, and H. Maring (2009b), Uncertainties in satellite remote sensing of aerosols and impact on monitoring its long-term trend: A review and perspective, *Ann. Geophys.*, *27*(7), 2755–2770.

Li, J., B. E. Carlson, and A. A. Lacis (2011), El Niño-Southern Oscillation correlated aerosol Ångström Exponent anomaly over the tropical Pacific discovered in satellite measurements, *J. Geophys. Res.*, *116*, D20204, doi:10.1029/2011JD015733.

Li, J., B. E. Carlson, and A. A. Lacis (2013a), Application of spectral analysis techniques in the intercomparison of aerosol data: 1. An EOF approach to analyze the spatial-temporal variability of aerosol optical depth using multiple remote sensing data sets, *J. Geophys. Res. Atmos.*, *118*, 8640–8648, doi:10.1002/jgrd.50686.

Li, J., B. E. Carlson, and A. A. Lacis (2013b), Application of different spectral analysis techniques in the inter-comparison of aerosols data part III: Using Combined PCA to compare spatio-temporal variability of MODIS, MISR and OMI aerosol optical depth, *J. Geophys. Res. Atmos.*, doi:10.1002/2013JD020538, accepted.

Liu, L., M. I. Mishchenko, I. Geogdzhayev, A. Smirnov, S. M. Sakerin, D. M. Kabanov, and O. A. Ershov (2004), Global validation of two-channel AVHRR aerosol optical thickness retrievals over the oceans, *J. Quant. Spectrosc. Radiat. Transfer*, *88*, 97–109, doi:10.1016/j.jqsrt.2004.03.031.

Lu, Z., D. G. Streets, Q. Zhang, S. Wang, G. R. Carmichael, Y. F. Cheng, C. Wei, M. Chin, T. Diehl, and Q. Tan (2010), Sulfur dioxide emissions China and sulfur trends in East Asia since 2000, *Atmos. Chem. Phys.*, *10*, 6311–6331, doi:10.5194/acp-10-6311-2010.

Mahowald, N. M., J. A. Ballantine, J. Feddema, and N. Ramankutty (2007), Global trends in visibility: Implications for dust sources, *Atmos. Chem. Phys.*, *7*(12), 3309–3339.

Martonchik, J. V., R. A. Kahn, and D. J. Diner (2009), Retrieval of Aerosol Properties over Land Using MISR Observations, in *Satellite Aerosol Remote Sensing Over Land*, edited by A. A. Kokhanovsky and G. de Leeuw, pp. 267–293, Springer, Berlin.

Mauldin, L. E., III, N. H. Zaun, M. P. McCormick Jr., J. H. Guy, and W. R. Vaughn (1986), Stratospheric aerosol and gas experiment II instrument: A functional description, *Opt. Eng.*, *24*(2), 242,307–242,307.

McCormick, M. P. (1987), SAGE II: An overview, *Adv. Space Res.*, *7*(3), 219–226.

Meehl, G. A., J. M. Arblaster, J. Y. Fasullo, A. Hu, and K. E. Trenberth (2011), Model-based evidence of deep-ocean heat uptake during surface-temperature hiatus periods, *Nat. Clim. Change*, *1*, 360–364.

Minnis, P., E. F. Harrison, L. L. Stowe, G. G. Gibson, F. M. Denn, D. R. Doelling, and W. L. Smith (1993), Radiative climate forcing by the Mount Pinatubo eruption, *Science*, *259*(5100), 1411–1415.

Mishchenko, M. I., and I. V. Geogdzhayev (2007), Satellite remote sensing reveals regional tropospheric aerosol trends, *Opt. Express*, *15*(12), 7423–7438.

Mishchenko, M. I., I. V. Geogdzhayev, B. Cairns, W. B. Rossow, and A. A. Lacis (1999), Aerosol retrievals over the ocean by use of channels 1 and 2 AVHRR data: Sensitivity analysis and preliminary results, *Appl. Opt.*, *38*(36), 7325–7341.

Mishchenko, M. I., I. V. Geogdzhayev, W. B. Rossow, B. Cairns, B. E. Carlson, A. A. Lacis, and L. D. Travis (2007), Long-term satellite record reveals likely recent aerosol trend, *Science*, *315*(5818), 1543–1543.

Mishchenko, M. I., L. Liu, I. V. Geogdzhayev, J. Li, B. E. Carlson, A. A. Lacis, B. Cairns, and L. D. Travis (2012), Aerosol retrievals from channel-1 and -2 AVHRR radiances: Long-term trends updated and revisited, *J. Quant. Spectrosc. Radiat. Transfer*, *113*, 1974–1980, doi:10.1016/j.jqsrt.2012.05.006.

Post, M. J., C. J. Grund, A. M. Weickmann, K. R. Healy, and R. J. Willis (1996), Comparison of Mount Pinatubo and El Chichon volcanic events: Lidar observations at 10.6 and 0.69 μm, *J. Geophys. Res.*, *101*(D2), 3929–3940, doi:10.1029/95JD02926.

Remer, L. A., et al. (2008), Global aerosol climatology from the MODIS satellite sensors, *J. Geophys. Res.*, *113*, D14S07, doi:10.1029/2007JD009661.

Rossow, W. B., and L. C. Garder (1993), Cloud detection using satellite measurements of infrared and visible radiances for ISCCP, *J. Clim.*, *6*(12), 2341–2369.

Rossow, W. B., and R. A. Schiffer (1999), Advances in understanding clouds from ISCCP, *Bull. Am. Meteorol. Soc.*, *80*, 2261–2288.

Russell, P. B., et al. (1996), Global to microscale evolution of the Pinatubo volcanic aerosol derived from diverse measurements and analyses, *J. Geophys. Res.*, *101*(D13), 18,745–18,763, doi:10.1029/96JD01162.

Solomon, S., J. S. Daniel, R. R. Neely, J. P. Vernier, E. G. Dutton, and L. W. Thomason (2011), The persistently variable "background" stratospheric aerosol layer and global climate change, *Science*, *333*(6044), 866–870.

Streets, D. G., Y. Wu, and M. Chin (2006), Two-decadal aerosol trends as a likely explanation of the global dimming/brightening transition, *Geophys. Res. Lett.*, *33*, L15806, doi:10.1029/2006GL026471.

Strong, A. E., and L. L. Stowe (1993), Comparing stratospheric aerosols from El Chichón and Mount Pinatubo using AVHRR data, *Geophys. Res. Lett.*, *20*(12), 1183–1186.

Thomason, L. W., S. P. Burton, B. P. Luo, and T. Peter (2008), SAGE II measurements of stratospheric aerosol properties at non-volcanic levels, *Atmos. Chem. Phys.*, *8*, 983–995.

Trepte, C. R., R. E. Veiga, and M. P. McCormick (1993), The poleward dispersal of Mount Pinatubo volcanic aerosol, *J. Geophys. Res.*, *98*(D10), 18,563–18,573, doi:10.1029/93JD01362.

Vernier, J.-P., et al. (2011), Major influence of tropical volcanic eruptions on the stratospheric aerosol layer during the last decade, *Geophys. Res. Lett.*, *38*, L12807, doi:10.1029/2011GL047563.

Wang, K., R. E. Dickinson, and S. Liang (2009), Clear sky visibility has decreased over land globally from 1973 to 2007, *Science*, *323*(5920), 1468–1470.

Wild, M. (2009), Global dimming and brightening: A review, *J. Geophys. Res.*, *114*, D00D16, doi:10.1029/2008JD011470.

Wild, M., H. Gilgen, A. Roesch, A. Ohmura, C. N. Long, E. G. Dutton, and A. Tsvetkov (2005), From dimming to brightening: Decadal changes in solar radiation at Earth's surface, *Science*, *308*(5723), 847–850.

Zhang, J., and J. S. Reid (2010), A decadal regional and global trend analysis of the aerosol optical depth using a data-assimilation grade over-water MODIS and Level 2 MISR aerosol products, *Atmos. Chem. Phys.*, *10*, 10,949–10,963, doi:10.5194/acp-10-10949-2010.

Zhao, T. X. P., I. Laszlo, W. Guo, A. Heidinger, C. Cao, A. Jelenak, and J. Sullivan (2008), Study of long-term trend in aerosol optical thickness observed from operational AVHRR satellite instrument, *J. Geophys. Res.*, *113*, D07201, doi:10.1029/2007JD009061.